CHEESA: Chemical Engineering Research Articles
ISSN 2614-8757 (Print), ISSN 2615-2347 (Online)
Homepage: https://e-journal.unipma.ac.id/index.php/cheesa

Research Article

OPEN ACCESS

CHEESA, 9(1), pp 1-14, 2026

Green Synthesis of CuO-Doped Fe_3O_4 for Degradation of Crystal Violet Dye: RSM-Based Optimization

Ady Mara[1)], Fahma Riyanti[1)], Desnelli[1)], Poedji Loekitowati Hariani[1*)]
[1)]*Universitas Sriwijaya, Department of Chemistry, Jl. Palembang Prabumulih, Ogan Ilir 30862, Indonesia*

*corresponding author: puji_lukitowati@mipa.unsri.ac.id

Article History

Submitted: 25th March 2026; Revised: 1st May 2026; Accepted: 11th May 2026;

Available online: 18th May 2026; Published Regularly: June 2026

doi: 10.25273/cheesa.v9i1.24394.1-14

Abstract

The limitations of CuO photocatalyst include high electron–hole recombination and low charge-transfer efficiency. In this context, doping with Fe_3O_4 is used to form a heterojunction, which enhances charge separation, increases electron transfer, and imparts magnetic properties for easy separation and reuse of the catalyst. Therefore, this study aimed to synthesize a biphasic CuO/Fe_3O_4 composite using *Rhodomyrtus tomentosa* leaf extract as a green reducing agent, and evaluate the performance as a photocatalyst for the degradation of Crystal Violet Dye (CVD). Structural, morphological, optical, and magnetic properties were characterized using X-ray diffraction (XRD), scanning electron microscopy with energy-dispersive X-ray spectroscopy (SEM–EDX), UV–Vis diffuse reflectance spectroscopy (DRS), and vibrating sample magnetometer (VSM). XRD patterns confirmed the coexistence of CuO and Fe_3O_4 phases, indicating successful composite formation. VSM analysis reported that the composite had magnetic properties with a saturation magnetization and band gap values of 46.92 emu/g and 1.63 eV, respectively. Process optimization was conducted using Response Surface Methodology (RSM) based on Central Composite Design (CCD). The results showed that the quadratic model was the most appropriate and statistically significant model, indicated by a p-value < 0.05 with a coefficient of determination (R^2) of 0.9902. In addition, optimization of the degradation process led to CVD degradation efficiency of 98.73% under optimal conditions of initial concentration of 25.4 mg/L, pH 9.5, and irradiation time of 39.4 min with a visible-light radiation source. The composite also reported good reusability, retaining 92.11% of degradation efficiency after five cycles, confirming the potential as a magnetically recoverable, environmentally sustainable photocatalyst for wastewater treatment applications.

Keywords: Crystal violet dye; CuO/Fe_3O_4 composite; quadratic model; *Rhodomyrtus tomentosa* leaf extract; RSM

1. Introduction

Rapid industrial development is driving economic growth and leading to various environmental problems, particularly the increasing volume and types of industrial waste [1]. Liquid waste from various industrial sectors contains organic and inorganic pollutant compounds, such as dyes, heavy metals, aliphatic hydrocarbons, polycyclic aromatic hydrocarbons, and benzene derivatives. In this context, the textile industry is a major contributor of dye-containing waste globally, with approximately 70% used being synthetic azo-based. These dyes are very stable, difficult to degrade naturally, and toxic to organisms [2]. During the process, approximately 10–15% of the dye does not bind to the fiber and is discarded as waste [3],[4]. At low concentrations (1 mg/L), some dyes can produce striking colors in aquatic environments, disrupting aesthetics and reducing water quality [3]. Crystal Violet Dye (CVD) is widely used in the textile industry with a stable molecular structure classified as a cation and carcinogen, causing serious impacts on human health and threatening aquatic ecosystems [5]. Existing wastewater treatment methods are often unable to effectively remove the contaminants. Therefore, more appropriate treatment strategies are needed to control the organic pollutants.

Photocatalytic degradation is considered more advantageous than conventional treatment methods to remove contaminants because the process mineralizes organic pollutants into harmless

This is an open access article under the CC BY license (http://creativecommons.org/licenses/by/4.0/)

end products, rather than transferring to another phase as occurs in adsorption or coagulation processes. CuO is a p-type semiconductor with a relatively narrow band gap in the range of 1.2–2.0 eV, enabling efficient absorption of visible light. Photocatalytic performance is superior to wide band gap semiconductors such as TiO_2 under visible-light irradiation [6]. The narrow band gap facilitates electron excitation under lower photon energy, promoting the generation of reactive oxygen species responsible for pollutant degradation. Furthermore, CuO is cost-effective and exhibits low toxicity [7]-[9]. The practical application as a photocatalyst is limited by the high electron–hole recombination rate and relatively poor stability under certain operating conditions. The potential leaching of Cu^{2+} ions restricts the environmental applications, necessitating modification with other semiconductors to enhance the stability and photocatalytic efficiency [6],[10].

Various studies have reported the development of CuO-based photocatalysts, including CuO/$MnFe_2O_4$ [10], Sr/CuO [11], CeO_2/CuO [12], and CuO–Ag [6]. Spinel-type ferrite materials with the general formula MFe_2O_4 (M = Co, Mn, Ni, Fe, and others) are recognized for high structural stability and intrinsic magnetic properties, contributing to enhanced photocatalytic performance and facilitating catalyst recovery. Among the ferrites, Fe_3O_4 is particularly attractive due to low cost, low toxicity, chemical stability, and ease of surface modification. The integration of photocatalytic activity with magnetic characteristics enables efficient post-treatment separation and improves reusability [13],[14]. Therefore, coupling Fe_3O_4 with CuO represents a rational strategy to mitigate the limitations of CuO. Fe_3O_4 is introduced as a promoter for charge transfer through the formation of a heterojunction with CuO. This interfacial interaction facilitates the separation of photogenerated charge carriers, enhancing photocatalytic efficiency.

Green synthesis method uses biological resources, including plant extracts, as reducing and stabilizing agents. This strategy offers several advantages, including lower environmental impact, improved biocompatibility, and greater cost-effectiveness compared to conventional synthetic routes [15],[16]. Bioactive compounds present in plant extracts play a crucial role in controlling nanoparticle nucleation and growth, influencing particle size and morphology. These phytochemicals also modify surface chemical properties and enhance colloidal stability through the introduction of functional groups onto the material surface [17]. *Rhodomyrtus tomentosa* (Ait.) Hassk. is a flowering plant thriving in diverse natural ecosystems, such as coastal zones, primary forests, wetlands, humid environments, and swamp margins [18]. This species is distributed across Southeast Asia, including Indonesia, and is locally known as karamunting or keramunting. Ethanol extracts of leaves contain various bioactive metabolites, such as flavonoids, phenolic compounds, tannins, and saponins [19]. Furthermore, the presence of alkaloids has also been reported by Kuntorini et al [20]. The phytochemical constituents function as reducing and stabilizing agents, influencing nucleation, particle size, and surface functionalization. These factors are critically correlated with improved interfacial contact in CuO–Fe_3O_4 heterojunction, enhanced charge separation, and higher photocatalytic activity.

This study reports the synthesis of CuO/Fe_3O_4 composite using *Rhodomyrtus tomentosa* leaf extract through the green method and the application in the photodegradation of CVD. Process optimization was conducted using Response Surface Methodology (RSM) to evaluate the effects of key operational variables and to determine the optimal degradation conditions. RSM facilitates the development of a predictive model that describes the relationship between process variables and photocatalytic efficiency. This reduces the number of experimental trials and allows the identification of optimal conditions with higher accuracy. Therefore, the use of RSM is essential to achieve a comprehensive understanding and to optimize the system efficiently.

2. Research Methods

2.1. Tools and Materials

Rhodomyrtus tomentosa leaves were collected from Ogan Ilir Regency, Indonesia. Iron(III) chloride hexahydrate ($FeCl_3.6H_2O$) (Merck), iron(II) chloride tetrahydrate ($FeCl_2.4H_2O$) (Merck), copper(II) chloride ($CuCl_2$) (Merck), sodium hydroxide (NaOH) (Merck), and Crystal Violet dye (Sigma-Aldrich) were used without further purification. Deionized water was adopted in all experiments.

Characterization of CuO/Fe_3O_4 composite was conducted utilizing several analytical methods. Phase identification was performed using X-ray diffraction (XRD, PANalytical) with Cu–Kα radiation (λ = 1.54107 Å) operated at 40 kV and 30 mA. Morphological features and elemental

composition were examined using scanning electron microscopy with energy-dispersive X-ray spectroscopy (SEM–EDX, FlexSEM 1000 II). Optical properties were evaluated by UV–Vis diffuse reflectance spectroscopy (DRS, Cary 60, version 2.00). Magnetic properties were measured using a vibrating sample magnetometer (VSM, Oxford 1.2H). The absorbance of dye solutions was analyzed using a UV–Vis spectrophotometer (Thermo Orion AquaMate 8000). Furthermore, functional group analysis was carried out using Fourier transform infrared spectroscopy (FTIR, Nicolet iS5) in the wavenumber range of 400–4000 cm^{-1}.

2.2. Preparation of Leaf Extract

The extraction procedure was adapted from Khoshsang et al [21]. Fresh *Rhodomyrtus tomentosa* leaves were thoroughly cleaned to remove surface impurities and washed several times with deionized water. A total of 500 g of leaves were air-dried at room temperature for 3 days and ground into a fine powder (±100 mesh). Approximately 10 g of leaf powder was added to a beaker containing 100 mL of deionized water, and the mixture was heated at 80°C for 1 h under continuous stirring. After cooling to room temperature, the solution was filtered using Whatman No. 1 filter paper (pore size 11 µm) to obtain leaf extract, which was used for subsequent synthesis.

2.3. Synthesis of CuO/Fe_3O_4 Composite

A total of 1.69 g $CuCl_2$ was dissolved in 50 mL of deionized water, and the mixture was stirred for 15 min. Subsequently, 25 mL of leaf extract was added while stirring continuously. A 1 M NaOH solution was added dropwise until the pH reached 10. The solution color changed from clear blue to dark black, indicating precipitate formation. The suspension was centrifuged at 9000 rpm for 10 min, and the collected precipitate was washed several times with deionized water. The obtained solid was calcined at 400°C for 2 h to produce CuO powder.

CuO/Fe_3O_4 composite was synthesized using the previously prepared CuO. The mass ratio of CuO and Fe_3O_4 is 1:1. Specifically, 1.12 g $FeCl_3.6H_2O$ and 0.41 g $FeCl_2.4H_2O$ were dissolved in 50 mL deionized water, followed by 25 mL leaf extract. The mixture was stirred for 15 min and heated to 60°C. 1 M NaOH was added dropwise until the pH reached 10 while maintaining constant stirring. The resulting suspension was centrifuged at 9000 rpm for 10 min, and the precipitate was collected and washed thoroughly with deionized water and ethanol. Finally, the product was dried at 70°C for 6 h to obtain CuO/Fe_3O_4 composite [16].

2.4. Photocatalytic Degradation Procedure

Photocatalytic degradation experiments were conducted using a batch system. In this study, RSM was used to optimize photocatalytic degradation, and data analysis was carried out through Design-Expert (version 13). RSM is a statistical and mathematical method used to plan experiments and analyze the influence of several independent variables on one or more response variables. Central Composite Design (CCD) was selected over Box–Behnken Design (BBD) due to greater flexibility in building quadratic models, and provided more complete information about the system behavior [22]. A total of three independent variables were investigated, namely initial CVD concentration (10, 30, and 50 mg L^{-1}), pH (4, 7, and 10), and irradiation time (30, 60, and 90 min). Furthermore, 100 mL of CVD solution was treated with 0.1 g of the catalyst. The reaction was carried out in a beaker placed inside a shaking incubator operating at 150 rpm under visible-light irradiation provided by a 400 W tungsten halogen lamp positioned at a distance of 15 cm. All experiments were performed at room temperature, and the absorbance of the solution after degradation was measured at 590 nm using a UV–Vis spectrophotometer.

3. Results and Discussion

3.1. Characterization of CuO/Fe_3O_4 Composite

As shown in Figure 1, the typical diffraction peaks of Fe_3O_4 appear at 2θ values of 30.10°, 35.62°, 43.34°, 53.46°, 57.10°, and 62.54°, which correspond to the (220), (311), (400), (422), (511), and (440) crystal planes, respectively. These peaks are in good agreement with the standard JCPDS card No. 19-0629, confirming the formation of crystalline magnetite (Fe_3O_4) with a cubic inverse spinel structure. The diffraction pattern reports the coexistence and partial overlap of CuO and Fe_3O_4 peaks for CuO/Fe_3O_4 composite. CuO reflections are observed at 2θ values of 32.20°, 35.60°, 38.72°, 48.22°, 53.50°, and 58.10°, consistent with JCPDS No. 89-2530 and confirming the monoclinic structure [23]. An overlap occurs in the 35–36° range, where Fe_3O_4 (311) and CuO (-111) reflections coincide to form a dominant peak. Variations in peak intensity and slight peak broadening may be attributed to the overlap of diffraction peaks from the two phases. Slight peak broadening and intensity

decrease were observed in green synthesis using *Rhodomyrtus tomentosa* leaf extract. The small peak shifts may be due to lattice strain and interactions with organic compounds from the extract. XRD results verify the successful formation of a biphasic CuO/Fe_3O_4 composite with well-defined crystalline structures.

SEM micrographs at a magnification of 5000× show that CuO/Fe_3O_4 composite exhibits an inhomogeneous surface morphology with particles distributed across the entire surface. Fe_3O_4 particles tend to form agglomerates with spherical morphology, while CuO particles report a more elongated and irregular shape. The agglomeration of Fe_3O_4 is mainly caused by magnetic forces, high surface energy, and van der Waals forces [22]. The coexistence of distinct morphological features leads to a relatively rough and heterogeneous surface texture, as shown in Figure 2. Elemental mapping obtained from SEM–EDX analysis suggests that Fe and Cu are distributed in the composite surface (Figure 3). CuO/Fe_3O_4 composite exhibited Fe, Cu, and O as the primary constituent elements. The presence of Fe and O corresponds to the Fe_3O_4 phase, while the Cu peak confirms the incorporation of CuO. The elemental composition of approximately 49% Fe, 38% Cu, and 13% O, and the absence of additional peaks, suggest that the synthesis process is successful and free of detectable impurity phases.

The band gap energy is a crucial parameter that determines a material's light absorption capability and directly influences photocatalytic performance. As shown in Figure 4(a), Fe_3O_4 and CuO/Fe_3O_4 exhibit absorption peak at 492 nm and 442 nm, indicating a shift in optical response after composite formation. Similar absorption characteristics have been reported for CuO synthesized using *Chlorella vulgaris* and *Gloriosa superba* extracts in the range of 280–410 nm [24] and 400–420 nm, respectively [25]. The optical band gap energy was estimated using the Tauc relation in Equation 1. hv represents photon energy, α is the absorption coefficient, E_g is direct band gap energy, and *k* is the proportionality constant.

$$\alpha hv = k(hv - E_g)^{1/2} \quad \text{.....(Equation 1)}$$

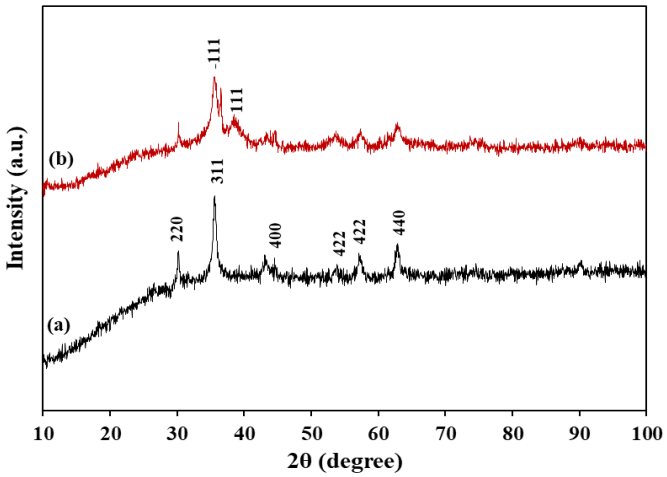


Figure 1. XRD pattern of (a) Fe_3O_4 dan (b) CuO/Fe_3O_4 composite

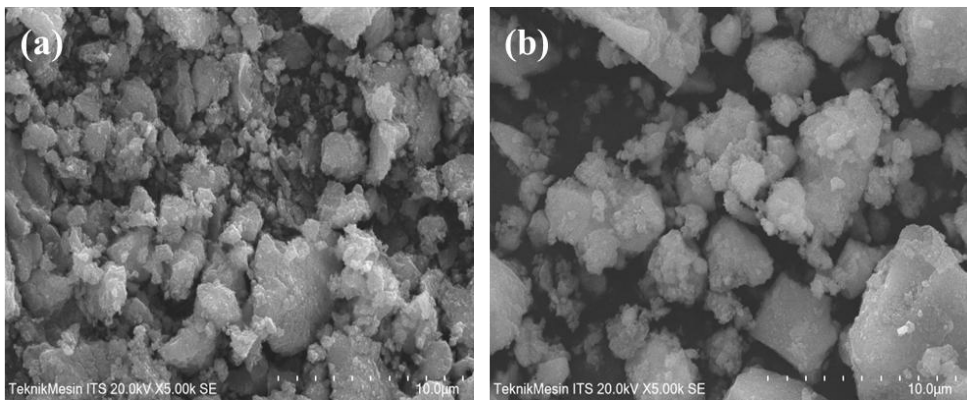


Figure 2. Surface morphology of (a) Fe_3O_4 and (b) CuO/Fe_3O_4 composite as observed by SEM analysis

CuO/Fe_3O_4 composite consists of two semiconductors with distinct band gap characteristics. The overall band structure is expected to differ from the individual components. As shown in Figure 4(b), the estimated band gap of CuO/Fe_3O_4 composite is 1.63 eV. This value is lower than Fe_3O_4 (2.05 eV) and falls in the reported range for CuO (1.2–2.0 eV) [7],[26]. The relatively narrow band gap enhances visible-light absorption, supporting efficient photocatalytic degradation under visible-light irradiation.

The hysteresis curve provides insight into the magnetic behavior of ferrite and composite materials. The magnetization–field (M–H) curve shown in Figure 5 exhibits an S-shaped profile, characteristic of ferromagnetic behavior. The synthesis route strongly influences the magnetic properties of ferrite materials. For example, Fe_3O_4 synthesized using *Moringa oleifera* leaf extract and *Prosopis farcta* extract exhibited Saturation Magnetization (Ms) values of 54 emu/g and 51.22 emu/g, respectively. Bulk Fe_3O_4 typically shows an Ms of approximately 92 emu/g [27].

In this present study, the measured Ms values for Fe_3O_4 and CuO/Fe_3O_4 composite were 76.18 emu/g and 46.92 emu/g, respectively. A comparable reduction in magnetization has been reported for CuO-modified $MnFe_2O_4$, where Ms value decreased from 53.7 emu/g to 23.3 emu/g after composite formation [10]. The use of plant extracts during synthesis and the incorporation of non-magnetic components contribute to a decline in overall magnetic strength due to surface effects and phase dilution [22],[27]. The formation of the CuO/Fe_3O_4 interface induces surface spin disorder and magnetic dead layers, where a significant fraction of atoms are located at or near the interface. This leads to a partial imbalance of magnetic spins, which lowers the saturation magnetization. Despite the decrease, CuO/Fe_3O_4 composite retains sufficiently strong magnetic properties to allow rapid and efficient separation from the reaction medium, facilitating catalyst recovery.

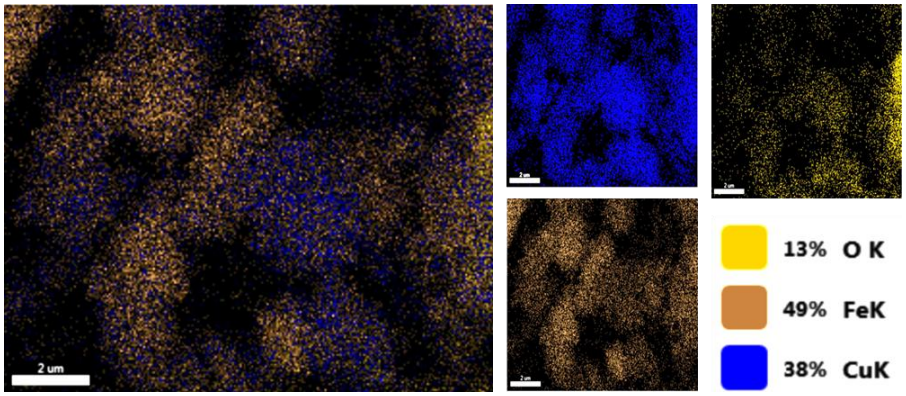


Figure 3. Elemental distribution of Fe, Cu, and O in CuO/Fe_3O_4 composite obtained from SEM mapping

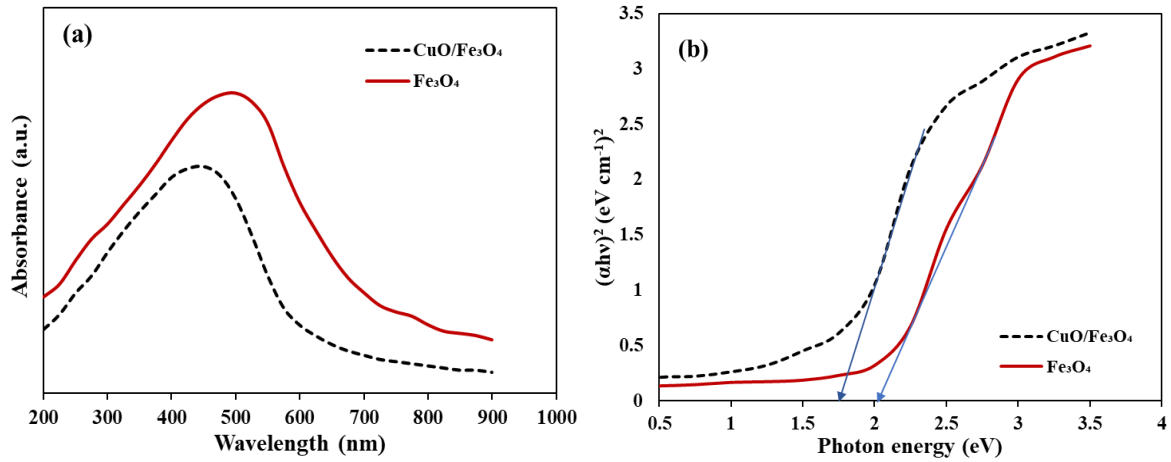


Figure 4. UV–Vis spectra (a) and Tauc plot analysis (b) for the determination of the optical band gap of Fe_3O_4 and CuO/Fe_3O_4 composite

3.2. Photocatalytic Optimization

Optimization of the photocatalytic degradation process was conducted by evaluating three principal variables, namely solution pH, initial dye concentration, and irradiation time. The effects and interactions of variables were analyzed using RSM based on CCD. The selection of the quadratic model was justified by an analysis of variance (ANOVA), where the model was statistically significant (p-value < 0.05). Table 1 summarizes the comparison between the experimental and predicted degradation efficiencies. The deviation (residual) between actual and predicted values ranges from 0.15 to 2.03, showing good agreement. The relatively small differences confirm the adequacy and predictive reliability of the proposed model. Furthermore, Figure 6 presents the correlation between actual and predicted CVD degradation efficiencies. The data points are distributed along the diagonal line, indicating strong conformity between experimental observations and model estimations.

ANOVA results in Table 2 show that the three main variables and interactions significantly influence degradation efficiency, as evidenced by p-values < 0.05. Highly significant effects ($p < 0.0001$) were observed for dye concentration, pH, and the interaction terms concentration–time, pH–time, and time-time, showing a dominant contribution to degradation response. The lack-of-fit test was not significant since the proposed quadratic model adequately represented the experimental data. Table 3 shows a statistical overview of model performance. The coefficient of determination (R^2) of 0.9953 reports that the model explains 99.53% of the total variation in CVD degradation efficiency. Adjusted R^2 (0.9910) and Predicted R^2 (0.9504) values are in close agreement, with a difference below 0.2, showing good model consistency and predictive capability. Adequate Precision value of 47.6804 exceeds the minimum required value of 4, confirming a strong signal-to-noise ratio. Therefore, the model has sufficient sensitivity to navigate the experimental design space effectively.

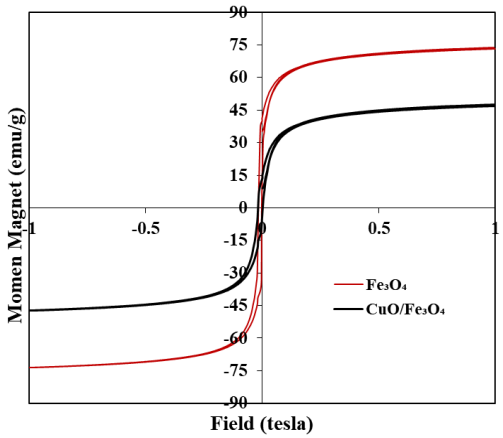


Figure 5. Magnetic hysteresis loops of Fe_3O_4 and CuO/Fe_3O_4 composite obtained from vibrating sample magnetometer (VSM) analysis at room temperature.

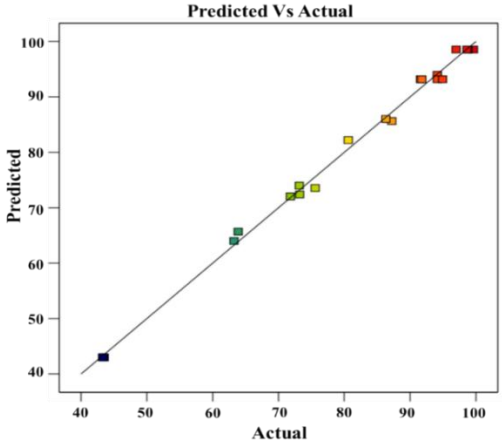


Figure 6. Diagnostic plots evaluating the predicted vs actual model value of degradation

Table 1. Difference in degradation efficiency of Crystal Violet Dye (CVD) between actual and predicted values

Run	CVD (mg/L)	pH	Irradiation time (min)	Response (%)		Residual
				Actual	Predicted	
1	50	4	90	73.21	72.38	0.83
2	50	7	30	87.22	85.64	1.58
3	30	7	60	94.14	93.12	0.96
4	10	7	60	86.31	86.01	0.29
5	30	7	90	75.58	73.55	2.03
6	50	7	90	63.88	65.69	-1.81
7	30	7	30	80.61	82.19	-1.58
8	30	7	60	91.56	93.18	-1.62
9	10	4	30	43.25	43.00	0.25
10	10	4	90	73.16	73.99	-0.83
11	10	4	30	43.51	43.00	0.51
12	30	10	60	96.99	98.55	-1.56
13	50	10	60	94.14	93.99	0.15
14	30	10	60	98.81	98.55	0.26
15	30	7	60	91.78	93.18	-1.39
16	30	7	60	94.94	93.18	1.76
17	30	10	60	98.62	98.55	0.067
18	30	10	60	99.64	98.55	1.087
19	50	4	30	63.24	63.99	-0.75
20	10	7	90	71.81	72.03	-0.22

Table 2. ANOVA for the quadratic model used in Crystal Violet Dye (CVD) degradation

Source	Sum of squares	Df	Mean square	F-value	p-value	
Model	5712.81	9	634.76	233.82	<0.0001	significant
A-Concentration	32.39	1	32.396	11.93	0.0062	
B-pH	199.13	1	199.136	73.35	<0.0001	
C-Time	76.64	1	76.64	28.23	0.0003	
AB	17.65	1	17.65	6.50	0.0289	
AC	208.36	1	208.37	76.75	<0.0001	
BC	418.27	1	418.28	154.08	<0.0001	
A^2	51.82	1	51.83	19.09	0.0014	
B^2	21.68	1	21.68	7.99	0.0180	
C^2	479.73	1	479.73	176.72	<0.0001	
Residual	27.15	10	2.71			
Lack of Fit	14.84	3	4.95	2.81	0.1172	not significant
Pure Error	12.30	7	1.76	233.82		
Cor Total	5736.96	19				

Table 3. Statistical overview of model performance

Parameters	Value
Standard Deviasi	1.65
Mean	81.12
C.V. %	2.03
R^2	0.9953
Adjusted R^2	0.9910
Predicted R^2	0.9504
Adeq Precision	47.6804

The contour plots and three-dimensional response surface graphs are presented in Figure 7. The curved profiles observed in the plots are characteristic of a quadratic model, confirming the presence of interaction effects among variables. Degradation efficiency initially increases with high dye concentration. However, the efficiency declines, as indicated by color gradient changes in the contour plot. This decrease is attributed to the shielding effect at higher dye concentrations, where excess dye molecules affect light penetration to the catalyst surface, reducing photon absorption and limiting the generation of reactive radicals [28].

The optimal pH was observed at approximately pH 9. Since CVD is a cationic dye, alkaline conditions favor degradation due to the negatively charged catalyst surface, which enhances electrostatic attraction and promotes dye adsorption.

Similar optimal conditions have been reported for CVD photodegradation at pH 9 and 11 using La-doped ZnO [29] and ZnS–Co_3O_4, respectively [2]. An increase in irradiation time leads to higher degradation efficiency due to prolonged exposure of the pollutant to reactive species such as •OH and $•O_2^-$ radicals generated on the catalyst surface. However, the RSM model indicates that the increase in degradation efficiency becomes less significant, suggesting a tendency toward equilibrium. This behavior is attributed to the progressive depletion of dye molecules and the possible accumulation of intermediate products that may compete for active sites on the catalyst surface. The optimum conditions predicted by RSM are derived from the curvature of the quadratic response surface, enabling the identification of the most favorable combination of operating variables [30].

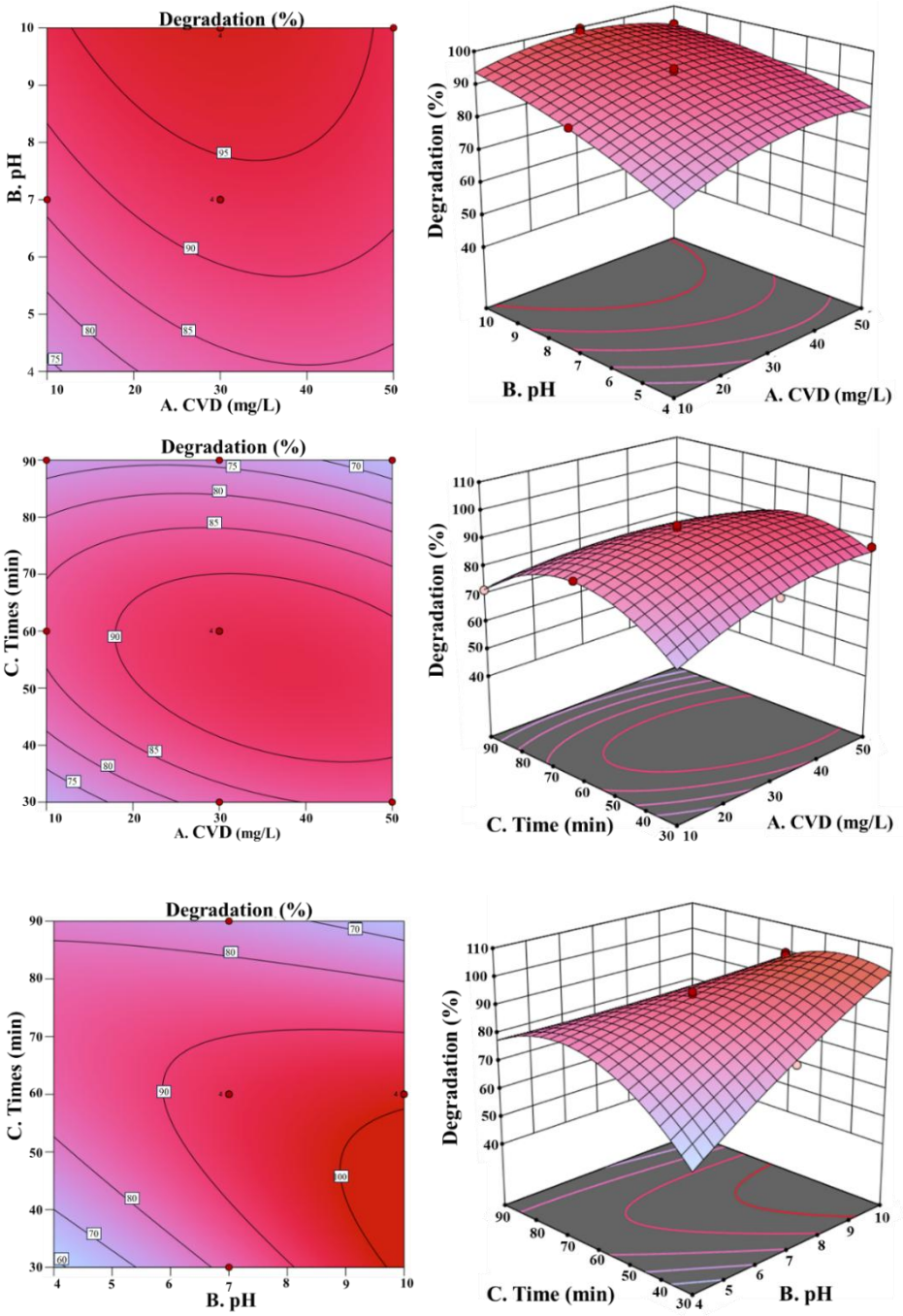


Figure 7. Contour and 3D response surface plots reporting the effects of process variables on photocatalytic degradation of Crystal Violet Dye (CVD) using CuO/Fe_3O_4 composite

The mathematical relationship between the independent variables and degradation efficiency was described using a quadratic model. The general form of the quadratic regression equation is expressed in Equation 2. The desirability function is used to evaluate how well a given combination of process variables satisfies the defined optimization criteria. A desirability value approaching 1 shows that the predicted conditions closely achieve the targeted objective, reflecting an optimal balance among the investigated variables. The optimal conditions obtained from model predictions are presented in Table 4, with manual optimization through experimental observations. RSM optimization predicts an optimal irradiation time of 39.4 min, significantly shorter than the 60 min used in the experimental condition. This reduction suggests the effectiveness of the statistical model in identifying more efficient operating.

CVD degradation efficiency reported superior performance compared to several previous studies. Photocatalytic degradation using Co_3O_4 nanoparticle photocatalyst was reported to achieve an efficiency of 92% at a concentration of 10 ppm with irradiation time of 45 min [31]. Meanwhile, the use of ZnO nanoparticles led to an efficiency of 95% at the same concentration with an irradiation time of 60 min [32].

3.3. Stability and Reusability of Catalyst

Stability and reusability are parameters in evaluating photocatalyst performance, particularly for reducing operational costs and enabling large-scale industrial applications. After each photocatalytic degradation run, the composite was separated from the mixture using an external magnet, washed thoroughly with ethanol and deionized water, and dried at 100°C for 1 h [33]. The recovered photocatalyst was reused for five consecutive cycles under the optimized conditions, leading to a decrease of 6.62% in degradation efficiency. The observed decrease in photocatalytic performance after repeated cycles was attributed to several deactivation mechanisms. The partial loss of active sites due to the adsorption of intermediate degradation products on the catalyst surface may block light absorption and affect the generation of reactive species. The decline may be attributed to partial catalyst loss during the magnetic separation and regeneration steps, consistent with previous reports [34].

$$\text{Degradation (\%)} = -94.92566 + 1.66775A + 16.63600B + 3.28160C - 0.039385AB - 0.009419AC - 0.157392CB - 0.011714A^2 - 0.248211B^2 - 0.017011C^2 \quad \textbf{.....(Equation 2)}$$

Table 4. Optimum conditions between experiments and optimization using RSM

Anaysis	[CVD] (mg/L)	pH	Time (min)	Degradation (%)
Experiment	30	10	60	98.55
RSM	25.4	9.5	39.4	98.73

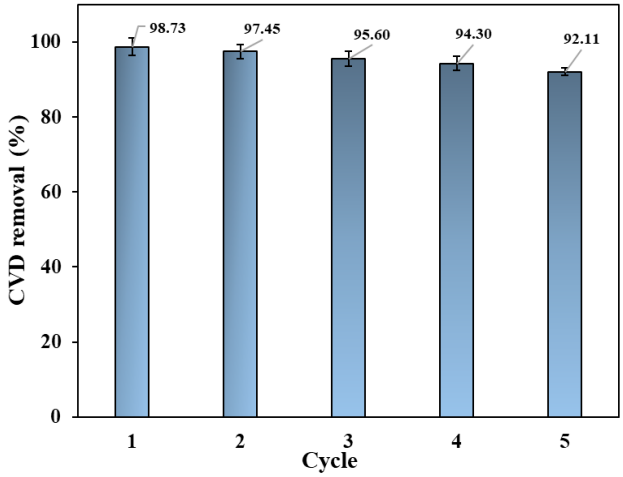


Figure 8. Reusability of CuO/Fe_3O_4 composite after photocatalytic degradation of Crystal Violet Dye (CVD)

Figure 9 presents FTIR spectra of CuO/Fe_3O_4 composite before and after the photocatalytic degradation process. The broad absorption band around 3400 cm^{-1} corresponds to the stretching vibration of hydroxyl (–OH) groups, which are attributed to surface hydroxyl species and adsorbed water molecules. Furthermore, the band in the region of 1600–1650 cm^{-1} is associated with O–H bending vibrations of adsorbed water or with aromatic C=C stretching vibrations derived from organic residues of leaf extract. Absorption band of 560–575 cm^{-1} is assigned to metal–oxygen (M–O) stretching vibrations, characteristic of Fe–O and Cu–O bonds [35].

The band near 1070 cm^{-1} may be attributed to C–N stretching vibrations originating from bioactive compounds in the green synthesis process [21]. Before degradation, the characteristic absorption bands are observed at 3429 cm^{-1}, 1624 cm^{-1}, and 574 cm^{-1}. After photocatalytic treatment, these bands exhibit slight shifts to 3406 cm^{-1}, 1614 cm^{-1}, and 568 cm^{-1}. The shifts in wavenumber and minor intensity changes after degradation suggest alterations in the local chemical environment of surface functional groups during photocatalysis. However, no significant structural changes are observed in line with the reported stability of CuO/Fe_3O_4 composite.

3.4 Kinetic Study

The pseudo-first order kinetic model commonly applied in photocatalytic degradation studies is derived from the Langmuir–Hinshelwood mechanism under conditions of low pollutant concentration and constant catalyst loading [4],[36]. The linearized pseudo-first-order equation is expressed in Equation 3. C_0 and C_t represent the initial and concentration of CVD at time t (mg L^{-1}), respectively, and k is the apparent reaction rate constant (min^{-1}).

$$ln\left(\frac{C_t}{C_0}\right) = -kt \qquad \text{.....(Equation 3)}$$

Figure 10 shows that R^2 is 0.9913, suggesting excellent agreement between the experimental data and the pseudo-first-order kinetic model. In this study, the k value is 0.0549 min^{-1}, showing rapid degradation of CVD. This is smaller compared to CVD degradation using $ZnS\text{-}Co_3O_4$ with a value of 0.0605 min^{-1} [2].

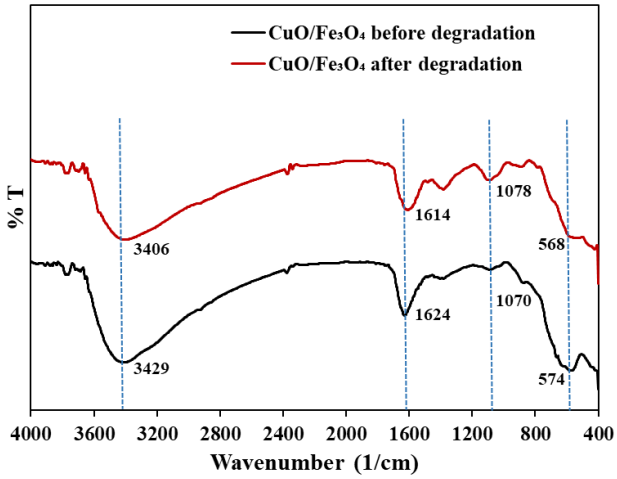


Figure 9. FTIR spectra of CuO/Fe_3O_4 composite before and after photocatalytic degradation

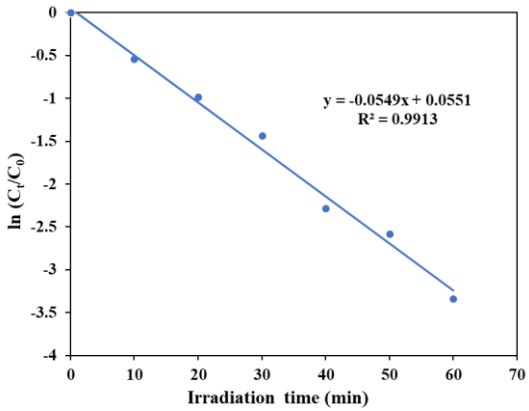


Figure 10. Pseudo-first order for photocatalytic degradation of Crystal Violet Dye (CVD) with Cuo/Fe_3O_4

Photocatalytic degradation of CVD by CuO/Fe_3O_4 composite occurs through the generation of electron–hole pairs under light irradiation, which produce reactive oxidative species such as •OH and $•O_2^-$ radicals. Figure 11 shows the CVD degradation scheme, while the mechanism is expressed in the Equation 4 [37],[38].

$$CuO/Fe_3O_4 + h\nu \rightarrow e_{CB}^- + h_{VB}^+$$
$$e_{CB}^- + O_2 \rightarrow •O_2^-$$
$$h_{VB}^+ + OH^- \rightarrow •OH$$
$$h_{VB}^+ + H_2O \rightarrow H^+ + •OH$$
$$•OH + •O_2^- + CVD \rightarrow H_2O + CO_2 + \text{other product} \quad \text{.....(Equation 4)}$$

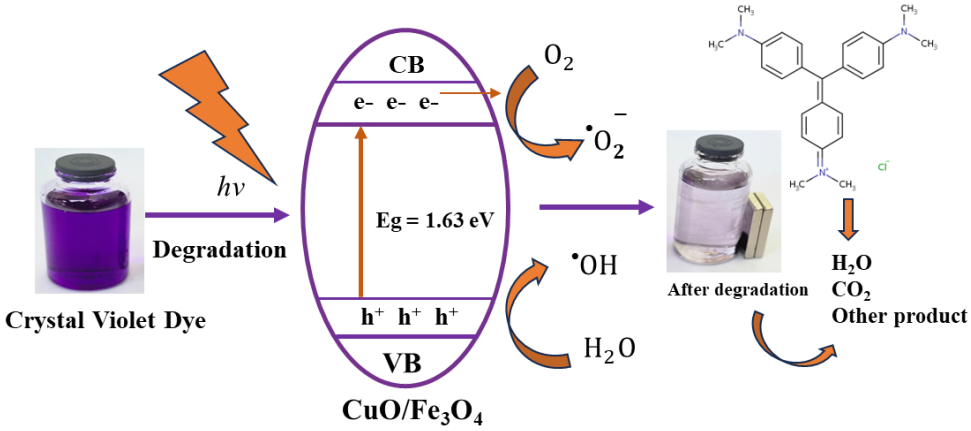


Figure 11. Photodegradation scheme of Crystal Violet Dye (CVD) with Cuo/Fe_3O_4

4. Conclusion

In conclusion, the superior photocatalytic performance of CuO/Fe_3O_4 composite was attributed to the synergistic effects arising from heterojunction formation, which enhances charge separation and visible-light utilization. The integration of *Rhodomyrtus tomentosa*-mediated green synthesis with a magnetically recoverable system showed a sustainable strategy for developing an efficient and reusable photocatalyst. Optimization of photocatalytic degradation using RSM identified significant effects of CVD concentration, pH, irradiation time, and the interactions on degradation efficiency. The optimum degradation efficiency (98.73%) according to the quadratic model was achieved at an initial concentration of 25.4 mg/L, pH 9.5, and irradiation time of 39.4 min. Kinetic evaluation also reported good agreement with the pseudo-first-order model at a rate constant of 0.0549 min^{-1}. After five reuse cycles, degradation efficiency decreased by 6.62% but remained above 90%. Future studies should focus on large-scale implementation, long-term stability, and the exploration of the system for wastewater treatment.

AI Usage Statements

The authors declare that no generative artificial intelligence (AI) tools were used in the writing, editing, analysis, or any part of the preparation of this manuscript. All content was conceived, written, and finalized solely by the authors without the assistance of AI technologies.

CRediT Authorship Statement

Ady Mara: Project administration, Conceptualization, and Supervision. **Fahma Riyanti**: Methodology, Formal analysis, and Data curation. **Desnelli**: Software, Validation, and Investigation. **Poedji Loekitowati Hariani**: Writing –Original draft, Writing-Review, and Visualization.

Declaration of competing interest

The authors declare there are no conflict of interest

Acknowledgments

The authors are grateful to Sriwijaya University for funding the 2025 fiscal year through a Competitive Scheme grant with contract No. 0108.167/UN9/SB3.LPPM.PT/2025, September 22, 2025.

References

[1] Ravi, A., Annamalai, P., Sankar, V., Achutharaman, K. R., Valdes, H., SaravanaVadivu, A., … Alharbi, S. A. (2024). Sustainable synthesis, superior performance: Nanoflower-like α-Bi_2O_3 from solvent-free solid state for photocatalytic Crystal violet degradation. *Journal of the Taiwan Institute of Chemical Engineers*, 157, 105413. doi: 10.1016/j.jtice.2024.105413

[2] Khan, S., Zeeshan, M., Jan, F. A., & Ullah, N. (2025). Photocatalytic degradation of Crystal violet and Eosin yellow dyes using ZnS-Co_3O_4 composite: Synthesis, characterization, and process optimization under UV light. *Inorganic Chemistry Communications*, 177, 114354. doi: 10.1016/j.inoche.2025.114354

[3] Tian, F., Wang, Y., Guo, G., Ding, K., Yang, F., Wang, H., … Liu, C. (2021). Enhanced azo dye biodegradation at high salinity by a halophilic bacterial consortium. *Bioresource Technology*, 326, 124749. doi: 10.1016/j.biortech.2021.124749

[4] Alwabsi, H. A. (2026). Cationic cellulose aerogel immobilized with horseradish peroxidase for visible light-assisted degradation and detoxification of Crystal violet dye. *Journal of the Taiwan Institute of Chemical Engineers*, 181, 106526. doi: 10.1016/j.jtice.2025.106526

[5] Neda, G., Taddesse, A. M., Diaz, I., Mohammed, A. M., Mayoral, Á., & Yassin, J. M. (2025). Nitrogen and phosphorus co-doped ZnO-CdO nanocomposite with boosted photocatalytic degradation of Crystal violet. *Scientific Reports*, 15(1). doi: 10.1038/s41598-025-01403-6

[6] Rathi, V. H., Jeice, A. R., & Jayakumar, K. (2023). Green synthesis of Ag/CuO and Ag/ TiO_2 nanoparticles for enhanced photocatalytic dye degradation, antibacterial, and antifungal properties. *Applied Surface Science Advances*, 18, 100476. doi: 10.1016/j.apsadv.2023.100476

[7] Raizada, P., Sudhaik, A., Patial, S., Hasija, V., Parwaz Khan, A. A., Singh, P., … Nguyen, V. H. (2020). Engineering nanostructures of CuO-based photocatalysts for water treatment: Current progress and future challenges. *Arabian Journal of Chemistry*, 13(11), 8424–8457. doi: 10.1016/j.arabjc.2020.06.031

[8] Liu, Q., Sun, J., Han, D., Liu, X., Gao, X., Jiang, Y., & Xie, K. (2020). Highly efficient photocatalytic removal of methylene blue by lamellar structured nanocrystalline and amorphous CuO. *Materials Letters*, 276, 128217. doi: 10.1016/j.matlet.2020.128217

[9] Gomaa, H., Zhai, Y., Wang, T., An, C., Lee, A., Deng, Q., & Hu, N. (2025). Morphology-performance relationship in hollow-sphere cobalt sulfide photocatalysts for solar-light-driven dye degradation: Integration of RSM, DFT, and machine learning. *Journal of Environmental Chemical Engineering*, 13(6), 119235. doi: 10.1016/j.jece.2025.119235

[10] Ma, Q., Zhang, H., Zhang, X., Li, B., Guo, R., Cheng, Q., & Cheng, X. (2019). Synthesis of magnetic CuO/$MnFe_2O_4$ nanocomposite and its high activity for degradation of Levofloxacin by activation of persulfate. *Chemical Engineering Journal*, 360, 848–860. doi: 10.1016/j.cej.2018.12.036

[11] Uma, H. B., Kumar, M. S. V., & Ananda, S. (2022). Semiconductor-assisted photodegradation of textile dye, photo-voltaic, and antibacterial property of electrochemically synthesized Sr-doped CuO nano photocatalysts. *Journal of Molecular Structure*, 1264, 133110. doi: 10.1016/j.molstruc.2022.133110

[12] Raees, A., Jamal, M. A., Ahmed, I., Silanpaa, M., & Algarni, T. S. (2021). Synthesis and characterization of CeO_2/CuO nanocomposites for photocatalytic degradation of Methylene blue in visible light. *Coatings*, 11(3), 11030305. doi: 10.3390/coatings11030305

[13] Mengting, Z., Kurniawan, T. A., Yanping, Y., Dzarfan Othman, M. H., Avtar, R., Fu, D., & Hwang, G. H. (2020). Fabrication, characterization, and application of ternary magnetic recyclable Bi_2WO_6/BiOI@Fe_3O_4 composite for photodegradation of Tetracycline in aqueous solutions. *Journal of Environmental Management*, 270, 126988. doi: 10.1016/j.jenvman.2020.110839

[14] Kumar, P., Deng, Z. Y., Tsai, P. Y., Chiu, C. Y., Lin, C. W., Chaudhary, P., … Chen, K. L. (2024). Enhanced visible-light photocatalytic activity of Fe_3O_4@MoS_2@Au nanocomposites for methylene blue degradation through Plasmon-Induced charge transfer. *Separation and Purification Technology*, 342, 126988. doi: 10.1016/j.seppur.2024.126988

[15] El-Sherbiny, G. M., Shehata, M. E., & Kalaba, M. H. (2025). Biogenic copper and copper oxide nanoparticles to combat multidrug-resistant *Staphylococcus aureus*: Green synthesis, mechanisms, resistance, and future perspectives. *Biotechnology Reports*, 46, e00896. doi: 10.1016/j.btre.2025.e00896

[16] Yizengaw, M. B., Kitaw, S. L., & Bekele, E. T. (2025). Green synthesis of CuO nanoparticles using *Rhamnus prinoides* leaf extracts, and mechanistic insights into antibacterial efficacy. *Journal of Agriculture and Food Research*, 24, 102481 doi: 10.1016/j.jafr.2025.102481

[17] Kandasamy, M., Husain, A., Pandian, S. A., Selvaraj, M., Suresh, S., Gunnasegaran, P., … Balaji, D. (2025). Greener and facile synthesis of binary zinc oxide/nickel oxide heterojunction nanocomposite for potential solar energy conversion, environmental remediation, and energy storage applications. *Results in Engineering*, 25, 103842. doi: 10.1016/j.rineng.2024.103842

[18] Zhao, Z., Wu, L., Xie, J., Feng, Y., Tian, J., He, X., … Zheng, X. (2020). *Rhodomyrtus tomentosa* (Aiton.): A review of phytochemistry, pharmacology, and industrial applications research progress. *Food Chemistry*. 309, 125715. doi: 10.1016/j.foodchem.2019.125715

[19] Puspito, S., Purwanto, P., Muhlisin, M., Kurniawati, A., Anggraeny, Y. N., Setiasih, S., … Krishna, N. H. (2024). Phytochemical diversity, rhodomyrtone content, nutrient content, and antioxidant efficacy in keramunting leaves from Belitung Island, Indonesia: A comparative study of different solvent extraction methods. *Case Studies in Chemical and Environmental Engineering*, 10, 100874. doi: 10.1016/j.cscee.2024.100874

[20] Kuntorini, E. M., Sari, S. G., & Fariani, R. (2023). The morphoanatomy, histochemistry, and phytochemistry of the leaves and fruits of *Rhodomyrtus tomentosa*. *Biodiversitas*, 24(1), 98–105. doi: 10.13057/biodiv/d240113

[21] Khoshsang, H., Abbasi, K., & Ghaffarinejad, A. (2023). Biosynthesis of ZnO and CuO nanoparticles using sunflower petal extract. *Inorganic Chemistry Communications*, 155, 111083. doi: 10.1016/j.inoche.2023.111083

[22] Denada, L., Aprianti, N., Philo, D., & Hariani, P. L. (2025). Eco-friendly synthesis of chitosan-PVA/Ag-CeO_2 composite for Crystal violet dye degradation and antibacterial performance. *Chimica Techno Acta*, 12(4), 9153. doi: 10.15826/chimtech.9153

[23] Fouad, S. S., Nabil, M., Horia, F., Easawi, K., & Negm, S. (2024). Synthesis of CuO/Fe_3O_4 Nanocomposite for enhanced solar thermal desalination. *Ceramics International*, 50(24), 54707–54715. doi: 10.1016/j.ceramint.2024.10.329

[24] Atri, A., Echabaane, M., Bouzidi, A., Harabi, I., Soucase, B. M., & Ben Chaâbane, R. (2023). Green synthesis of copper oxide nanoparticles using *Ephedra Alata* plant extract and a study of their antifungal, antibacterial activity and photocatalytic performance under sunlight. *Heliyon*, 9(2), 13484. doi: 10.1016/j.heliyon.2023.e13484

[25] Naika, H. R., Lingaraju, K., Manjunath, K., Kumar, D., Nagaraju, G., Suresh, D., & Nagabhushana, H. (2015). Green synthesis of CuO nanoparticles using *Gloriosa superba* L. extract and their antibacterial activity. *Journal of Taibah University for Science*, 9(1), 7–12. doi: 10.1016/j.jtusci.2014.04.006

[26] Abrar, M. M., Kabir, A., & Nishat, S. S. (2022). A DFT+U study on the structural, electronic, magnetic, and optical properties of Fe and Co co-doped CuO. *Materials Today Communications*, 32. doi: 10.1016/j.mtcomm.2022.103923

[27] Yew, Y. P., Shameli, K., Miyake, M., Ahmad Khairudin, N. B. B., Mohamad, S. E. B., Naiki, T., & Lee, K. X. (2020). Green biosynthesis of superparamagnetic magnetite Fe_3O_4 nanoparticles and biomedical applications in targeted anticancer drug delivery system: A review. *Arabian Journal of Chemistry*. 12(4), 1–13. doi: 10.1016/j.arabjc.2018.04.013

[28] Mohanty, L., Sundar Pattanayak, D., Singhal, R., Pradhan, D., & Kumar Dash, S. (2022). Enhanced photocatalytic degradation of rhodamine B and malachite green employing $BiFeO_3$/g-C_3N_4 nanocomposites: An efficient visible-light photocatalyst. *Inorganic Chemistry Communications*, 138, 109286. doi: 10.1016/j.inoche.2022.109286

[29] Raina, I., Kumar, P., Kumar, A., Singh, K., Somvanshi, A., Sawini, … Kumar, D. (2025). Visible-light-activated La-doped ZnO photocatalysts for enhanced degradation of Crystal violet dye. *Ceramics International*. 51, 54185–54199. doi: 10.1016/j.ceramint.2025.09.158

[30] Riyanti, F., Hariani, P. L., Hasanudin, H., Rachmat, A., & Purwaningrum, W. (2024). Optimization Photodegradation of Methylene Blue Dye using Bentonite/PDA/Fe_3O_4@CuO Composite by Response Surface Methodology. *Bulletin of Chemical Reaction Engineering and Catalysis*, 19(2), 252–264. doi: 10.9767/bcrec.20132

[31] Saravan, R. S., Muthukumaran, M., Mubashera, S. M., Abinaya, M., Prasath, P. V., Parthiban, R., … Sagadevan, S. (2020). Evaluation of the photocatalytic efficiency of cobalt oxide nanoparticles towards the degradation of Crystal violet and Methylene violet dyes. *Optik*, 207, 164428. doi: 10.1016/j.ijleo.2020.164428

[32] Pandey, B., Tewatia, H., Meel, D., & Singh, P. (2023). Phyto-fabrication of zinc oxide nanoparticles using Ficus religiosa and its potential application in the degradation of crystal violet dye. *Applied Chemical Engineering*, 6(3), 1–11. doi: 10.24294/ace.v6i3.2024

[33] Pakzad, K., Alinezhad, H., & Nasrollahzadeh, M. (2019). Green synthesis of Ni@Fe_3O_4 and CuO nanoparticles using *Euphorbia maculata* extract as photocatalysts for the degradation of organic pollutants under UV-irradiation. *Ceramics International*, 45(14), 17173–17182. doi: 10.1016/j.ceramint.2019.05.272

[34] Niaz, R., Sabir, M., Abid, M. Z., Mahar, J., Younas, U., Khan, M. A., … Hussain, E. (2025). Insight into the synthesis and proceeding of Ni-Al@Si–TiO_2 catalyst: A state-of-the-art approach for crystal violet dye degradation. *Surfaces and Interfaces*, 74, 107658. doi: 10.1016/j.surfin.2025.107658

[35] Kaur, K., Yamini, S., J V, R., G, L., Kumar, P., Rao K C, V., & Senapati, S. (2025). Green synthesis of saponin-capped copper (II) oxide (CuO) nanoparticles and their efficacy in photocatalytic dye degradation. *Sustainable Chemistry One World*, 6, 100054. doi: 10.1016/j.scowo.2025.100054

[36] Eddy, N. O., Jibrin, J. I., Ukpe, R. A., Odiongenyi, A., Iqbal, A., Kasiemobi, A. M., … Runde, M. (2024). Experimental and theoretical investigations of photolytic and photocatalysed degradations of crystal violet dye (CVD) in water by oyster shells-derived CaO nanoparticles (CaONP). *Journal of Hazardous Materials Advances*, 13, 100413. doi: 10.1016/j.hazadv.2024.100413

[37] Boucherdoud, A., Kherroub, D. E., Dahmani, K., Douinat, O., Seghier, A., Bestani, B., & Benderdouche, N. (2024). Polyaniline/cupric oxide organometallic nanocomposites as a sonocatalyst for the degradation of Methylene blue: Experimental study, RSM optimization, and DFT analysis. *Journal of Organometallic Chemistry*, 1022, 123386. doi: 10.1016/j.jorganchem.2024.123386

[38] Lee, Y. S., Lee, K. M., & Ong, B. H. (2025). Magnetic recoverable cobalt ferrite nanophotocatalyst for Crystal violet dye degradation. *Ceramics International*, 51, 39630–39638. doi: 10.1016/j.ceramint.2025.06.198